RESEARCH PAPER

# Mathematical model for IP$_3$ dependent calcium oscillations and mitochondrial associate membranes in non-excitable cells

## Neeraj Manhas [ID] [1,*,‡]

[1]Department of Mathematics, National Institute of Technology Raipur, Chhattisgarh, 492010, India
[*] Corresponding Author
[‡] nmanhas.maths@nitrr.ac.in (Neeraj Manhas)

## Abstract

Theoretical studies on calcium oscillations within the cytosolic [Ca$^{2+}$], and mitochondria [Ca$^{2+}$]$_{mit}$ have been conducted using a mathematical model-based approach. The model incorporates the mechanism of calcium-induced calcium release (CICR) through the activation of inositol-trisphosphate receptors (IPR), with a focus on the endoplasmic reticulum (ER) as an internal calcium store. The production of 1,4,5 inositol-trisphosphate (IP$_3$) through the phospholipase $C$ isoforms and its degradation via Ca$^{2+}$ are considered, with IP$_3$ playing a crucial role in modulating calcium release from the ER. The model includes a simple kinetic mechanism for mitochondrial calcium uptake, release and physical connections between the ER and mitochondria, known as mitochondrial associate membrane complexes (MAMs), which influence cellular calcium homeostasis. Bifurcation analysis is used to explore the different dynamic properties of the model, identifying various regimes of oscillatory behavior and how these regimes change in response to different levels of stimulation, highlighting the complex regulatory mechanisms governing intracellular calcium signaling.

**Keywords**: Mitochondria-associated membranes; Hopf bifurcation; periodic doubling bifurcation; calcium oscillation
**AMS 2020 Classification**: 34C23; 92B99; 92-10

## 1 Introduction

Calcium (Ca$^{2+}$) contributes to the vast array of various physiology and pathophysiology. The extremely rapid increase in cytosolic Ca$^{2+}$ leads to a multitude of cellular responses, such as release of neurotransmitters, muscle contraction, gene transcription, and cell proliferation [1–4]. Although the fluctuations observed in cytoplasmic Ca$^{2+}$ provided valuable insights into the complexity of Ca$^{2+}$ signaling. However, the toolkit involved in these regulations has a very fine control over its

components. However, non-excitable cells exhibit $Ca^{2+}$ oscillations of different frequencies and amplitudes on hormone stimulation [5–7]. These $Ca^{2+}$ oscillations are meticulously controlled by a network of receptors, pumps, exchangers, $Ca^{2+}$-ATPase, etc. The ER has IPR on its membrane. They released $Ca^{2+}$ on activation. Intracellular $IP_3$ binds to IPR with $Ca^{2+}$ as a co-agonist and opens them. Active IPR mediates the CICR process that enhances cytosolic $Ca^{2+}$. Physiologically low $Ca^{2+}$ concentrations are required for cell function. Thus, $Ca^{2+}$ is quickly pumped back into the ER lumen through $Ca^{2+}$ ATPase pumps from the sarco / endoplasmic reticulum (SERCA). It is also sent to the extracellular medium by $Ca^{2+}$ ATPase pumps (PMCA). Mitochondria uptakes $Ca^{2+}$ via uniporter (MCU). It releases $Ca^{2+}$ into the cytosol via the $Na^+/Ca^{2+}$ exchanger (NCX). Moreover, the direct flow of $Ca^{2+}$ ions occurs from the ER to the mitochondria through MAMs [8, 9].

Mathematical models are powerful tools for advancing scientific knowledge. However, models have an attractive ability to make experimentally testable predictions. In the field of $Ca^{2+}$ dynamics, researchers develop foundational models based on the available data, facilitating $Ca^{2+}$ dynamics within cells. Initially, models were built that have the capability to produce $Ca^{2+}$ oscillations at constant $IP_3$. For example: to understand rhythmic $Ca^{2+}$ fluctuations, a one-pool model is developed. It includes IPR activation both by $Ca^{2+}$ and constant $IP_3$ [10]. Atri et al. [11] constructed a biphasic form of the IPR channel, which produces $Ca^{2+}$ oscillation at constant $IP_3$. Few advanced models of this kind are seen here [12–14]. However, several models pointed out that the activation of $IP_3$ metabolism by $Ca^{2+}$ could lead to oscillations in $IP_3$. These models helped to clarify how changes in $Ca^{2+}$ levels might affect the dynamics of $IP_3$ and cause cells to oscillate. Models of these types are shown here [15, 16]. Furthermore, theoretically, the modelling approaches show that $Ca^{2+}$ oscillations occur in different types of cells: like acinar cells [17–20], hepatocytes [21–23], oocytes [24–26], cardiac myocytes [27–29], neuron [30, 31], fibroblast [32], etc. Regardless of the cell type, mitochondria are necessary for cells to survive [33–35]. Specialized subdomains or MAM, exist in the ER closest to mitochondria. It facilitates the entry of $Ca^{2+}$ ions and lipids into the mitochondria. The physical connection between mitochondria and the ER is quantitatively investigated here [36]. Marhl et al., [37] model served as the framework for that one. It is assumed that MCU perceives $Ca^{2+}$ are thought to be the MAM and the cytosol. Moreover, Moshkforoush et al., [38] Wacquier et al., [39], and Han and Periwal [40] developed models demonstrating $Ca^{2+}$ dynamics oscillations are influenced by ER mitochondrial micro-domains.

However, this article proposes a class II mathematical model for the $Ca^{2+}$ exchange between the cytosol and mitochondria. Experiments with exchangers, uniporters, pumps, $Ca^{2+}$ ATPase, $IP_3$ dynamics, and IPR validate the model's major components. The goal of this research is to understand the role of MAMs in non-excitable cells. The deterministic modeling technique utilized in this study gives information on the complex $Ca^{2+}$ flow via MAMs and other $Ca^{2+}$ compartments such as the cytosol, ER, and mitochondria, as well as how these routes influence the $Ca^{2+}$ response of each compartment individually. In short, modeling the physiology of non-excitable cells is an effective tool for understanding the relationships outlined above. This study is useful because it provides a comprehensive description of $Ca^{2+}$ signaling in non-excitable cells such as pancreatic acinar cells, hepatocytes, vascular endothelial cells, etc. Overall, this study seeks to analyze the experimental patterns anticipated by the predictions, revealing the process by which agonist concentration turns fundamental rhythmic patterns into complex oscillatory patterns.

The format for the rest of the paper's body is as follows: Following the introduction in Section 1, Section 2 covers the $Ca^{2+}$ toolkit's primary components and describes how to construct the model and create the mathematical equations. Section 3 presents the model's numerical analysis and

outcomes once it has been developed. The argument, conclusions drawn from the model's results, and any potential repercussions are then covered in Section 4.

## 2 The mathematical model of the problem

This paradigm explains $Ca^{2+}$ release mechanisms in the cytosol, endoplasmic reticulum, and mitochondria, using symbols $[Ca^{2+}]$, $[Ca^{2+}]_{er}$, and $[Ca^{2+}]_{mit}$. It considers fast $Ca^{2+}$ absorption, mitochondrial release, $IP_3$ generation, degradation, fluxes, leaks, and direct $Ca^{2+}$ exchange from the ER to mitochondria. Then the nonlinear kinetic equations are shown as follows:

$$
\begin{aligned}
\frac{d[Ca^{2+}]}{dt} &= (J_{IPR} + J_{ER}) - J_{SERCA} + \delta(J_{IN} - J_{PM}) + J_{NCX} - J_{MCU} - J_{RaM}, \\
\frac{d[Ca^{2+}]_{er}}{dt} &= \gamma(-(J_{IPR} + J_{ER}) + J_{SERCA} - J_{MAM}), \\
\frac{d[IP_3]}{dt} &= J_{IP_3 prod} - J_{IP_3 deg}, \\
\frac{d[Ca^{2+}]_{mit}}{dt} &= \tau(J_{MCU} + J_{RaM} - J_{NCX} + J_{MAM}).
\end{aligned}
\tag{1}
$$

In this model, $\delta$ controls the overall calcium flow via plasma membrane, cytoplasm volume to ER volume ratio is $\gamma$, and mitochondria volume to cytoplasm volume is $\tau$. The model is solved numerically and analyzed using AUTO [41] and MATLAB 2021b. Also, all the parameters' values are shown in Table 1.

### The IPR

The IPR is divided into six states: resting (R), activated (A), shut (S), open (O), and two inactivated ($I_1$), and ($I_2$) states. There are four components that make up the IPR. Two binding sites for $Ca^{2+}$ activation, one for $Ca^{2+}$ inactivation, and one for $IP_3$ are present in each subunit. $Ca^{2+}$ and $IP_3$ mediate the shift between these states. Consequently, the model equations provided for all states are given below. A thorough explanation of the model is here [42]

$$
\begin{aligned}
\frac{dR}{dt} &= \phi_{-2}O - \phi_2[IP_3]R + (k_{-1} + l_{-2})I_1 - \phi_1 R, \\
\frac{dO}{dt} &= \phi_2[IP_3]R - (\phi_{-2} + \phi_4 + \phi_3)O + \phi_{-4}A + k_{-3}S, \\
\frac{dA}{dt} &= \phi_4 O - \phi_{-4}A - \phi_5 A + (k_{-1} + l_{-2})I_2, \\
\frac{dI_1}{dt} &= \phi_1 R - (k_{-1} + l_{-2})I_1, \\
\frac{dI_2}{dt} &= \phi_5 A - (k_{-1} + l_{-2})I_2.
\end{aligned}
\tag{2}
$$

Here, $R, O, A, I_1, I_2$ denotes the fraction of receptors in the respective states, and $R + S + O + A + I_1 + I_2 = 1$. All $\phi$'s that are the functions of $[Ca^{2+}]$ are as follows:

$$
\begin{aligned}
\phi_1[Ca^{2+}] &= \frac{(k_1 L_1 + l_2)[Ca^{2+}]}{L_1 + [Ca^{2+}](1 + \frac{L_1}{L_3})}, \\
\phi_2[Ca^{2+}] &= \frac{k_2 L_3 + l_4[Ca^{2+}]}{L_3 + [Ca^{2+}](1 + \frac{L_3}{L_1})},
\end{aligned}
$$

$$\phi_{-2}[Ca^{2+}] = \frac{k_{-2} + l_{-4}[Ca^{2+}]}{(1 + \frac{Ca^{2+}}{L_5})},$$

$$\phi_3[Ca^{2+}] = \frac{k_3 L_5}{L_5 + [Ca^{2+}]},$$

$$\phi_4[Ca^{2+}] = \frac{(k_4 L_5 + l_6)[Ca^{2+}]}{L_5 + [Ca^{2+}]}, \tag{3}$$

$$\phi_{-4}[Ca^{2+}] = \frac{L_1(k_{-4} + l_{-6})}{L_1 + [Ca^{2+}]},$$

$$\phi_5[Ca^{2+}] = \frac{(k_1 L_1 + l_2)[Ca^{2+}]}{L_1 + [Ca^{2+}]}.$$

The open probability of the IPR is taken to be $P_{IPR} = (0.1O + 0.9A)^4$, thus, the calcium flux from the IPR is given as:

$$J_{IPR} = k_{IPR} P_{IPR}([Ca^{2+}]_{er} - [Ca^{2+}]). \tag{4}$$

### The SERCA pump and Ca$^{2+}$ ATPase pump (PMCA)

Calcium enters the ER via the SERCA pump, with the quasi-hill form model representing the pump flux, influenced by the ER's calcium content [43]

$$J_{SERCA} = V_{SERCA} \frac{[Ca^{2+}]}{K_{SERCA} + [Ca^{2+}]} \times \frac{1}{[Ca^{2+}]_{er}}. \tag{5}$$

Here, $V_{SERCA}$, $K_{SERCA}$ are the maximum permeability and half saturation constant of the SERCA pump, respectively. $Ca^{2+}$ is moved from the cytosol to the extracellular medium by the PMCA. As a result, the flow from the cytosol to the extracellular pool is expressed as (4):

$$J_{PM} = V_{PM} \frac{[Ca^{2+}]^2}{K_{PM}^2 + [Ca^{2+}]^2}. \tag{6}$$

Here, $V_{PM}$ is the permeability of the PMCA, and the $K_{PM}$ is a half-saturation constant. When calcium reaches the cytosol, the intracellular calcium is altered. The $J_{IN}$ is modeled as a function of increasing agonist concentration, with agonist-dependent inflow ($\alpha_2 V_{PLC}$) and constant leak ($\alpha_1$)

$$J_{IN} = \alpha_1 + \alpha_2 v_{PLC}. \tag{7}$$

Calcium leakage from the ER to the cytoplasmic $J_{ER}$ is directly linked to the variation in calcium concentrations.

### The IP$_3$ dynamics

PLC, whose activity is influenced by Ca2+ and agonist dosage, produces IP$_3$. The expression for the phospholipase C isoform production, also known as PLC$\beta$, and its Ca$^{2+}$ sensitivity is as follows [44]

$$J_{IP_3 prod} = V_{PLC} \frac{[Ca^{2+}]^2}{K_{PLC}^2 + [Ca^{2+}]^2}. \tag{8}$$

In this case, $K_{PLC}$ represents the sensitivity of PLC to calcium, while $V_{PLC}$ indicates the maximum synthesis rate of PLC isoforms. Next, the following kinetic equation for $IP_3$ degradation modulated by $[Ca2+]$ is given as

$$J_{IP_3deg} = k_{deg}\left(\frac{[Ca^{2+}]^2}{K_{deg}^2 + [Ca^{2+}]^2}\right)[IP_3],$$
(9)

where $K_{deg}$ is the $IP_3$ half saturation constant, and $k_{deg}$ describes the phosphorylation rate. The rate of variation of the cytosolic concentration of ($IP_3$) is therefore given as

$$\frac{d[IP_3]}{dt} = J_{IP_3prod} - J_{IP_3deg}.$$
(10)

### The mitochondrial uptake and release

The exchange of $Ca^{2+}$ between the cytosol and mitochondria occurs as the mitochondria absorb $Ca^{2+}$. The equation is as follows

$$J_{MCU} = k_{mcu}\frac{[Ca^{2+}]^2}{K_{mcu}^2 + [Ca^{2+}]^2}.$$
(11)

The $K_{mcu}$ is a half-activation constant, while the maximal permeability is $k_{mcu}$. The fast mode also removes $Ca^{2+}$ from the cytosol, therefore this exchange is provided by

$$J_{RaM} = k_{RaM}\frac{[Ca^{2+}]^8}{K_{RaM}^8 + [Ca^{2+}]^8}.$$
(12)

Here $k_{RaM}$ is the maximal permeability, and $K_{RaM}$, is the half-activation constant for the rapid mode.

### The $Na^+/Ca^{2+}$ exchanger

Within the mitochondria, the $Na^+/Ca^{2+}$ exchanger facilitates the gradual release of $Ca^{2+}$. The exchanger for it is provided as

$$J_{NCX} = v_{NCX}\frac{[Na^+]_{cyto}^3}{k_{Na}^3 + [Na^+]_{cyto}^3}\frac{[Ca^{2+}]_{mit}}{k_{NCX} + [Ca^{2+}]_{mit}}.$$
(13)

The $Na^+/Ca^{2+}$ exchanger's activation constants are $k_{Na}$ and $k_{NCX}$, with the cytosolic $Na^+$ concentration being $[Na^+]_{cyto}$, and its maximal activity being $V_{NCX}$.

### Mitochondrial-Associated Membranes (MAMs)

The ER and mitochondria are physically connected to form stanch structural domains known as mitochondria-associated ER membranes. It participates in fundamental biological $Ca^{2+}$ homeostasis processes. Further, the evidence is, that there is a physical contact between ER $Ca^{2+}$ release sites and mitochondrial $Ca^{2+}$ uptake sites [45]. Thus, the $Ca^{2+}$ flux from ER to mitochondria

directly is given by

$$J_{MAM} = k_{MAM_1} \frac{[Ca^{2+}]_{er}^2}{K_{MAM_1}^2 + [Ca^{2+}]_{er}^2} + k_{MAM_2} \frac{[Ca^{2+}]_{er}^8}{K_{MAM_2}^8 + [Ca^{2+}]_{er}^8}, \quad (14)$$

where $k_{MAM_1}$, $k_{MAM_2}$ are the maximal permeability and $K_{MAM_1}$, $K_{MAM_2}$ are the half-activation constants for the $J_{MAM}$ fluxes.

## 3 Results: model analysis

Nonlinear differential Eqs. (1)-(2) in the system determine the dynamic behavior of the model and solve the system of equations numerically. A partial bifurcation analysis of the model is also carried out. The maximum PLC isoform synthesis rate is represented by the parameter $V_{PLC}$. This parameter, thus, serves as the model's bifurcation parameter.

The bifurcation diagram for $[Ca^{2+}]$ in Figure 1 illustrates how $V_{PLC}$ affects this. In this case, HB1 and HB2 represent the two Hopf Bifurcations. The stable periodic orbits are shown by dark black lines, and the unstable ones are shown by dark blue lines. Period doubling bifurcation point is depicted by PDs. TRs is an acronym for the tour's split point. The inset shows the period of oscillations. Steady-state stability decreases as $V_{PLC}$ rises. The steady state, for positive $V_{PLC}$ values $\approx 2.344$ to $34.4$ $\mu$M/s, contains two Hopf bifurcation points: right-most Hopf bifurcation (HB2) and left-most Hopf bifurcation (HB1). Hopf bifurcation arises when the steady state changes the stability. It causes the appearance or disappearance of a periodic orbit.
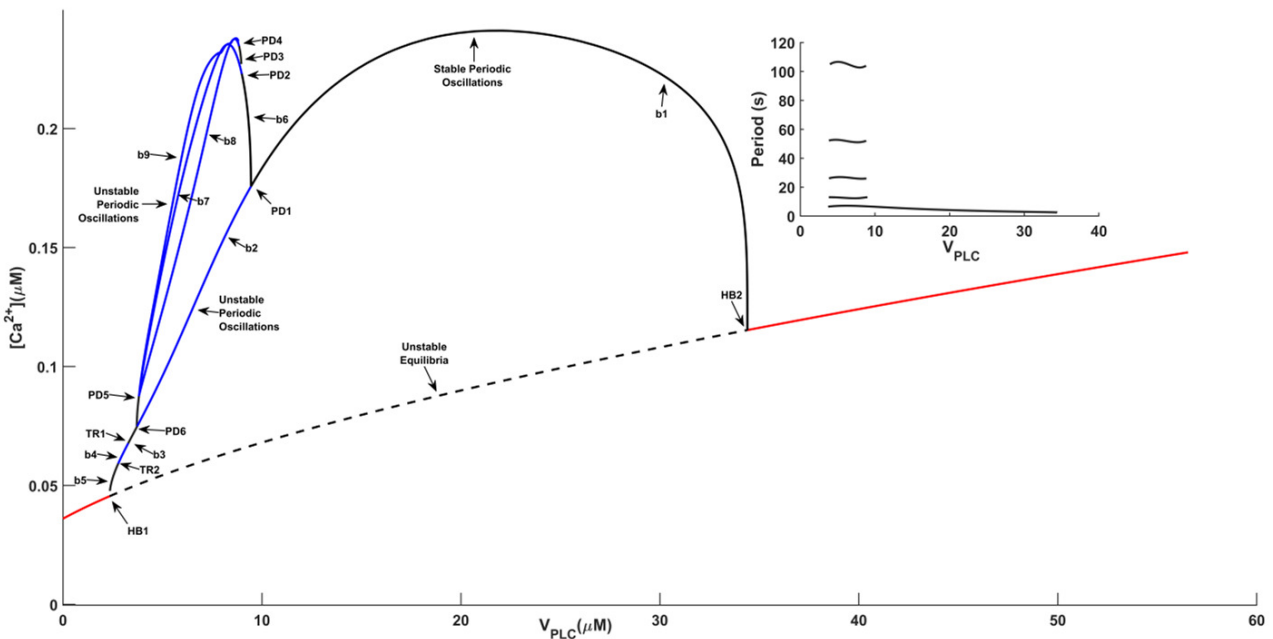


**Figure 1.** The maximum values of the periodic orbits with respect to $V_{PLC}$ are shown on the bifurcation diagram

Thus, the model enables oscillations between two $V_{PLC}$ values, with stable and unstable periodic oscillations. The steady state is the saddling node type. The stable branch b1 starts at HB2 at $V_{PLC}$ = $34.4$ $\mu$M/s and ends at PD1 at $V_{PLC} \approx 9.449$ $\mu$M/s, with oscillation periods ranging from $2.465$ to $6.526$ seconds.

Beginning at PD6, the tiny stable branch b3 stops at the point TR1 $V_{PLC} \approx 3.267\mu$M/s. The oscillation period of this little branch is $6.526$ to $6.245$ seconds. After that, the new unstable branch
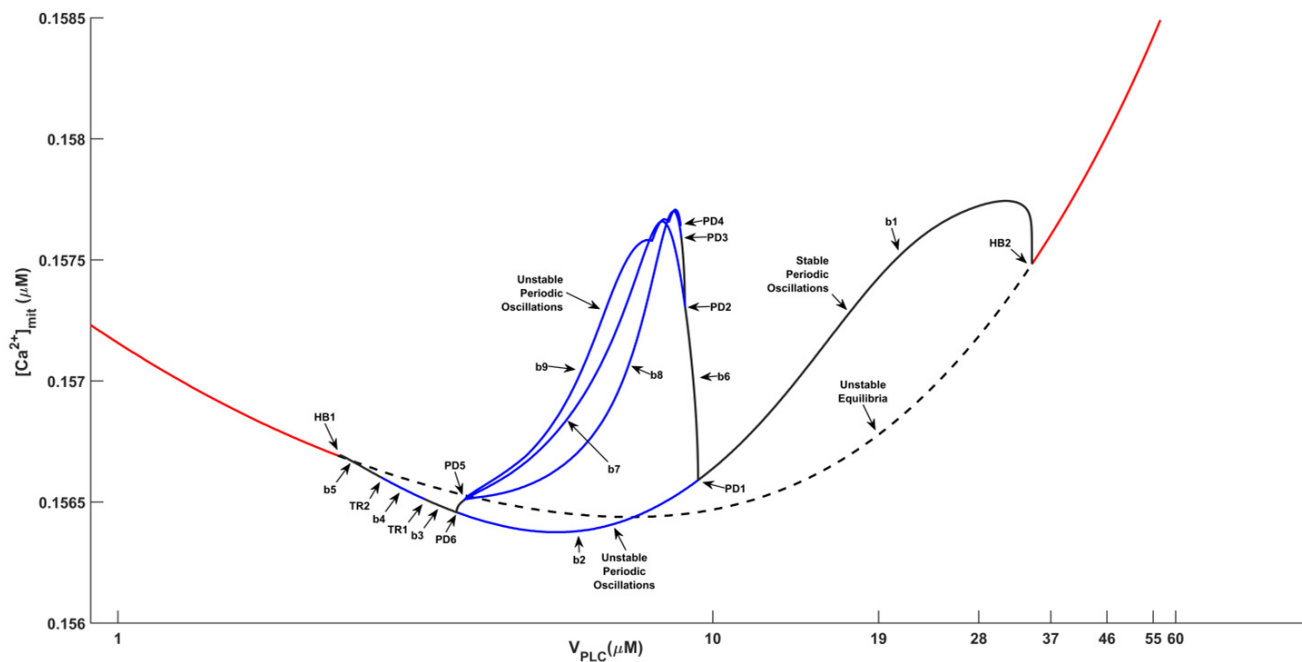
**Figure 2.** The bifurcation diagram of $[Ca^{2+}]_{mit}$ as a function of $V_{PLC}$

b4 blue line begins at tour point TR1 (3.267 $\mu$M/s) and finishes at TR2 $V_{PLC} \approx 2.777\mu$M/s. In this branch, oscillations occur approximately 6.245 to 5.447 seconds. Next, a little, stable branch called b5 (a solid black line) emerged from TR2 and ended close to HB1. On this branch, the oscillation period varies from approximately 5.853 to 5.447 seconds.

Starting at PD1 and ending at PD2, the new stable branch has a $V_{PLC}$ of roughly 13.05$\mu$M/s. At PD5, at $V_{PLC} \approx 3.854$ $\mu$M/s, the elongation from PD2 (branch b7) comes to a halt. At $V_{PLC} \approx 8.966$ $\mu$M/s, branch b7 has the PD3. Starting at PD3, the branch b8 ends at PD5. This branch oscillates at a period of roughly 26.07 to 26.11 seconds. The unstable branch b9 ends near PD5 and starts at $V_{PLC} \approx 8.816\mu$M/s, originating from PD4. The oscillation period of this branch is 51.98 to 52.21 seconds.

Figure 2 displays the bifurcation diagram that forecasts how $V_{PLC}$ will affect $[Ca^{2+}]_{mit}$. The dotted black lines are unstable equilibrium. The solid black lines represent the stable periodic orbits and dark blue lines represent the unstable periodic orbits. The PDs are the period-doubling bifurcation points. TRs represents the tours bifurcation point. Bifurcation points such as the Hopf bifurcation, period doubling, and Tours points happen at the same $V_{PLC}$ values as they do in Figure 1. As a result, both the stable and unstable branches in Figure 1 and Figure 2 correspond to oscillations whose period and amplitude fall within a scientifically meaningful range. The function of $V_{PLC}$ drives these complex dynamics both in cytosol and mitochondria. It should be mentioned that IP$_3$ fluctuations in this scenario are the cause of the $[Ca^{2+}]$ oscillations, that lead to $[Ca^{2+}]_{mit}$ oscillations.

$Ca^{2+}$ oscillations are more than just a biological curiosity; they have a substantial impact on cell function. Calcium signals indicate how cells can encode information in the frequency and amplitude of oscillations generated by their oscillatory nature. Thus, it is important to understand the dynamics of time series. Following that, the next several values of $V_{PLC}$ are displayed along with the distinct dynamic profiles of $[Ca^{2+}]$, $[Ca^{2+}]_{mit}$, and $[IP_3]$ oscillations.

The time series is periodic at PD3, $V_{PLC} \approx 8.853\mu$M, with a period of 26.01 seconds. Figure 3A, Figure 3C illustrates the oscillation of the $[Ca^{2+}]$ and $[Ca^{2+}]_{mit}$ time series, which exhibit four spikes in total: two large and two minor spikes. Furthermore, the $[IP_3]$ profile is displayed in
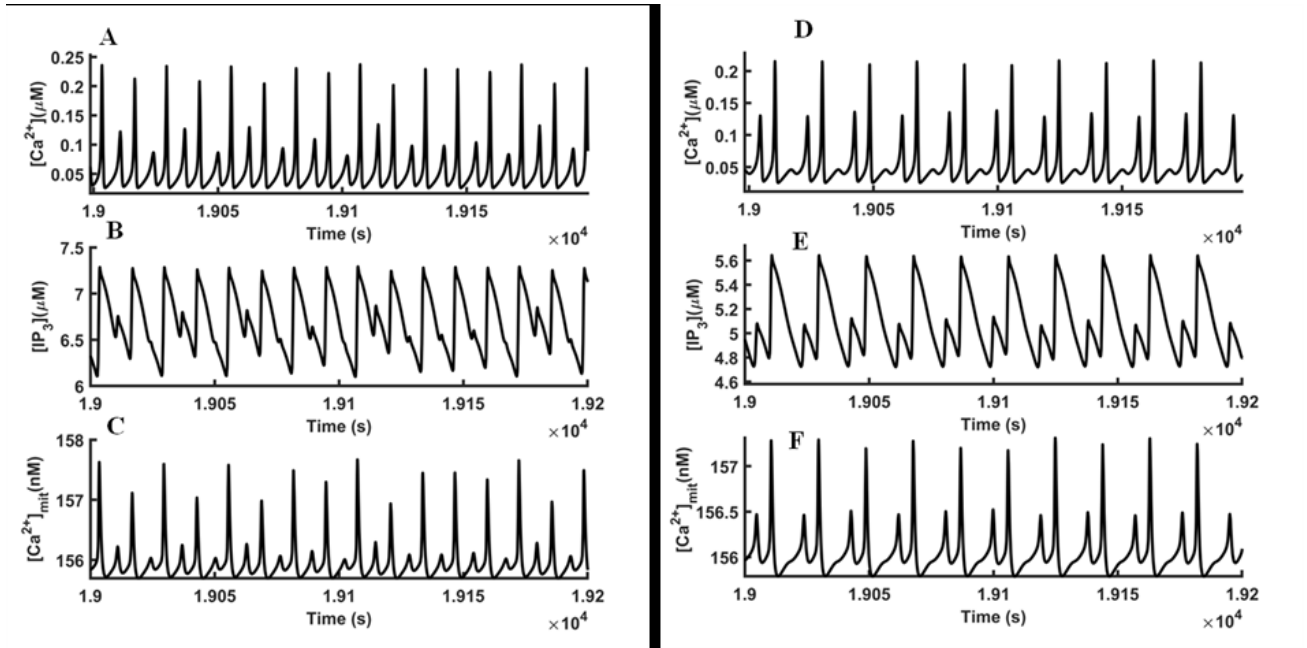
**Figure 3.** The time series profiles of $[Ca^{2+}]$, $[IP_3]$, and $[Ca^{2+}]_{mit}$ at $V_{PLC} = 8.853\mu M/s$, and $V_{PLC} = 7\mu M/s$, are shown in Panels A, B, and C and Panels D, E, F, respectively

Figure 3B. Three distinct attractors can be found in phase space at $V_{PLC} \approx 8.853\mu M$, When the stable periodic orbits reach the period-doubling bifurcation PD3, a powerful attractor is created. Additionally, there are two additional period doubling bifurcations (PD2 and PD4) that form complex attractors close to PD3. Consequently, there are variations in the amplitudes of the oscillations in $[IP_3]$, $[Ca^{2+}]$, and $[Ca^{2+}]_{mit}$ and. Figure 1 illustrates how it results from the merger of various attractors in the phase plane. Moreover, branch b7 exhibits a two-peak oscillation of $[Ca^{2+}]$ at $V_{PLC} = 7\mu M$, with a huge spike coming first, and a smaller spike following, as depicted in Panel D. In addition, the $[Ca^{2+}]_{mit}$ oscillates, showing two peaks in Panel F. Panel E displays the $[IP_3]$ pattern.

The predicted time series for $[Ca^{2+}]$ and $[Ca^{2+}]_{mit}$ exhibit two abrupt spikes with different small amplitudes at PD6, $V_{PLC} = 3.819 \mu M/s$, as illustrated in Figure 4A and Figure 4C, respectively. The unstable periodic orbits that merge into the stable periodic orbits, as seen in Figure 1 and Figure 2, complicate the $[Ca^{2+}]$ profile. Moreover, two bifurcation points PD5 and TR1 (torus point) exit near the PD6 area, which results in complex oscillations. TR1 occurs at $V_{PLC} = 3.267\mu M$. Figure 4D illustrates the smaller oscillations of $[Ca^{2+}]$ and $[Ca^{2+}]_{mit}$ having multiple large and small fluctuations having periods of around 6.245 seconds, respectively. When comparing the $Ca^{2+}$ profile in Figure 4E with Figure 4A, the $Ca^{2+}$ oscillates with less amplitude.

Furthermore, steady oscillations develop when $V_{PLC}$ is increased (see branch b1 of Figure 1 and Figure 2). When compared to unstable oscillations, stable oscillations have amplitudes that are comparable. Figure 5A and Figure 5C show that the $[Ca^{2+}]$ and $[Ca^{2+}]_{mit}$ oscillate with significant amplitudes and identical spikes at $V_{PLC} = 20\mu M$. Similar amplitude spikes are also shown in Figure 5B of the $[IP_3]$. Comparing Figure 5 panels Figure 5D, Figure 5E, and Figure 5F with Figure 5A, Figure 5B, and Figure 5C for $[Ca^{2+}]$, $[IP_3]$, and $[Ca^{2+}]_{mit}$ oscillations, respectively, reveals sinusoidal oscillations at $V_{PLC} = 30\mu M$, but the oscillations are also stable at this point. Approximately 2.5 seconds make up the oscillation period. Calcium oscillations with varying amplitudes at smaller frequencies are predicted by the model to be observed when $V_{PLC}$ is modest. Higher $V_{PLC}$ causes higher frequency oscillations. The oscillations in the $[IP_3]$ concentration are by $Ca^{2+}$ induced $IP_3$ production and degradation. However, the $IP_3$ plays a key role in the
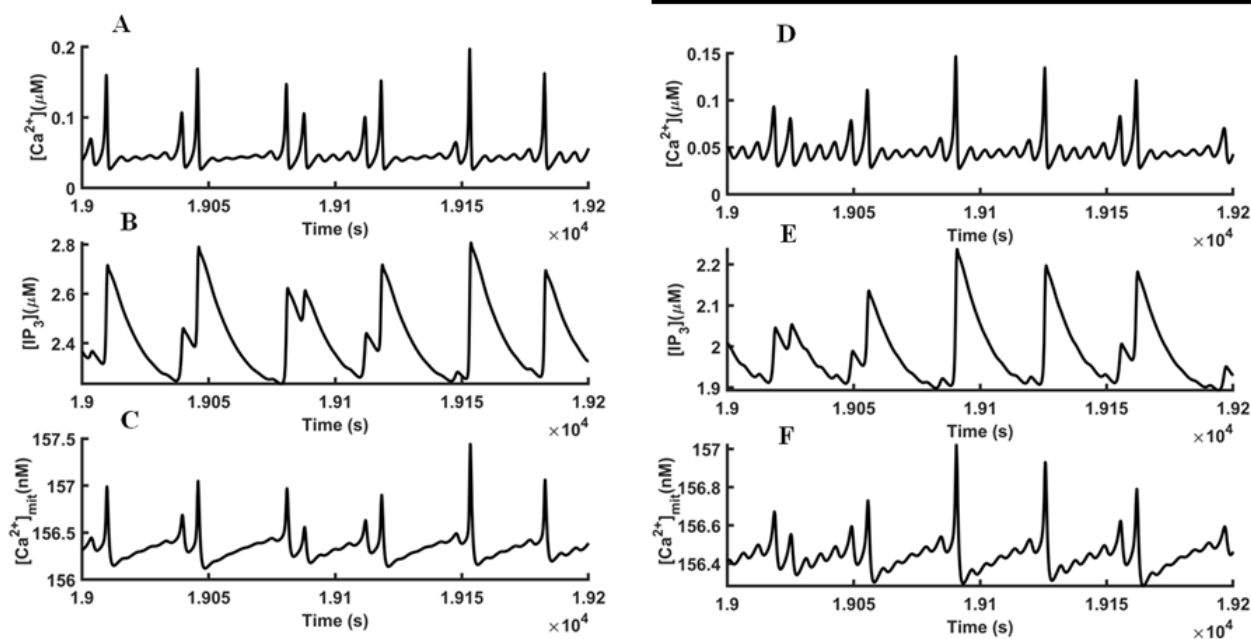
**Figure 4.** Qualitative oscillation behavior at different agonist concentrations, presenting time series profiles of $[Ca^{2+}]$, $[IP_3]$, and $[Ca^{2+}]_{mit}$ at $V_{PLC} = 3.819$ $\mu M/s$ (Panels A, B, C) and $3.267$ $\mu M/s$, (Panels D, E, F), respectively
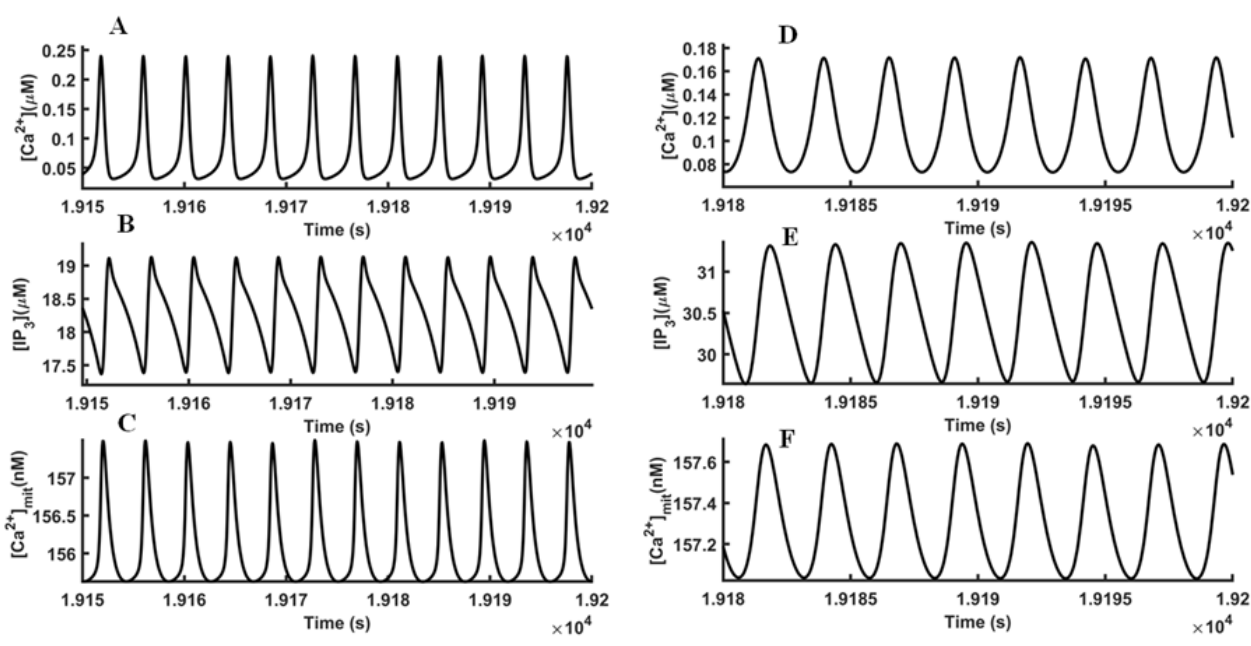


**Figure 5.** Numerical integration of agonist $V_{PLC}$ at different concentrations, displaying time series profiles of $[Ca^{2+}]$, $[IP_3]$, and $[Ca^{2+}]_{mit}$ at $20\mu M/s$ (Panels A, B, and C) and $30\mu M/s$ (D, E, and F)

modulation of $[Ca^{2+}]$ oscillations.

## 4  Discussion and conclusions

The goal of this study is to comprehend sophisticated $Ca^{2+}$ oscillations in the mitochondria and the cytoplasm. Agonist stimulations that cause CICR through IPR entrenched in the ER membrane elicit the calcium transients. Consideration is given to the cytosolic $IP_3$ synthesis by PLC and its degradation by $Ca^{2+}$. Through uniporters and the rapid mode mechanism, $Ca^{2+}$ is swiftly

Table 1. Parameter values used in the model taken from [17, 18, 20, 46]

| IPR Parameters values | | | | | |
|---|---|---|---|---|---|
| $k_1$ | 0.64 $(\mu M)^{-1}s^{-1}$ | $k_{-1}$ | 0.04 s$^{-1}$ | $l_2$ | 1.7 s$^{-1}$ |
| $k_2$ | 37.4 $(\mu M)^{-1}s^{-1}$ | $k_{-2}$ | 1.4 s$^{-1}$ | $l_4$ | 1.7 s$^{-1}(\mu M)^{-1}$ |
| $k_3$ | 0.11 $(\mu M)^{-1}s^{-1}$ | $k_{-3}$ | 29.8 s$^{-1}$ | $l_6$ | 4707 s$^{-1}$ |
| $k_4$ | 4.0 s$^{-1}(\mu M)^{-1}$ | $k_{-4}$ | 0.54 s$^{-1}$ | $L_1$ | 0.12 $\mu M$ |
| $L_3$ | 0.025 $(\mu M)$ | $L_5$ | 54.7 $\mu M$ | | |
| **IP$_3$ Parameters values** | | | | | |
| $K_{PLC}$ | 0.2 $\mu M$ | $k_{deg}$ | 0.5 s$^{-1}$ | $K_{deg}$ | 0.1 $\mu M$ |
| **Calcium Parameters** | | | | | |
| $k_{IPR}$ | 0.71 s$^{-1}$ | $J_{ER}$ | 0.002 s$^{-1}$ | $\delta$ | 0.1 |
| $\gamma$ | 5.405 | $\tau$ | 1.64 | $V_{SERCA}$ | 120 $(\mu M)^{-2}s^{-1}$ |
| $K_{SERCA}$ | 0.18 $\mu M$ | $V_{PM}$ | 28 $\mu Ms^{-1}$ | $K_{PM}$ | 0.425 $\mu M$ |
| $\alpha_1$ | 0.2 $(\mu M)s^{-1}$ | $\alpha_2$ | 0.05 s$^{-1}$ | | |
| **Mitochondrial Parameters** | | | | | |
| $k_{mcu}$ | 15 $(\mu M)s^{-1}$ | $K_{mcu}$ | 20 $\mu M$ | $k_{RaM}$ | 30 $(\mu M)s^{-1}$ |
| $K_{RaM}$ | 0.8 $\mu M$ | $V_{NCX}$ | 60 $(\mu M)^{-1}s^{-1}$ | $K_{NCX}$ | 35 $\mu M$ |
| $K_{Na}$ | 9.4 $\mu M$ | $[Na^+]_{cyto}$ | 10 $\mu M$ | $k_{MaM1}$ | 0.03 $(\mu M)s^{-1}$ |
| $K_{MaM1}$ | 20 $\mu M$ | $k_{MaM2}$ | 0.12 $(\mu M)s^{-1}$ | $K_{MaM2}$ | 1.8 $\mu M$ |

taken up by mitochondria and released slowly via an exchanger back into the cytosol. Cellular organelles, including mitochondria and ER, play distinct biological roles, physically forming MAMs and not being isolated entities, despite evidence suggesting otherwise [9]. MAMs are a dynamic interface that connects the outer mitochondrial membrane (OMM), the ER subdomain, and several proteins, serving as a link between the ER and mitochondria [47]. It helps the material and information flow between the ER and the mitochondria including Ca$^{2+}$ ions [45]. Thus, a straightforward but reliable mathematical model is developed to comprehend the intricacy of Ca$^{2+}$ dynamics, which includes direct Ca$^{2+}$ flow from the ER to the mitochondria, pumps, standard Ca$^{2+}$ fluxes, and the IP$_3$ metabolism that is associated IPR controls over activation and inactivation.

The bifurcation analysis is performed on the constructed model. The bifurcation analysis reveals the dynamical structures, that govern the oscillations (Figure 1). The existence of such unstable oscillations holds the fact that they exist for very small regions (blue dark lines) as shown in Figure 1 and Figure 2. The stable Ca$^{2+}$ oscillations exist for large regions (black dark lines) discussed above in Figure 1 and Figure 2. As predicted the model shows transient from simple to complex Ca$^{2+}$ oscillations. The model suggests that even at low levels of stimulation, the Ca$^{2+}$ response may exhibit erratic spikes. The Ca$^{2+}$ oscillations remain at high frequency and low amplitude even at large agonist dosages (Figure 2, Figure 3, Figure 4, Figure 5). Moreover, the correlation between agonist and oscillations period indicates that the period sharply decreases as stimulus concentration rises (see the inset in Figure 1). It is also observed that when the model is simulated without MAMs and mitochondrial dynamics. Bifurcation's dynamical structure ([Ca$^{2+}$] vs. $V_{PLC}$) differs significantly (results not shown). With few stable and unstable branches, the oscillations happen in the $V_{PLC}$ border range. These oscillations have large amplitudes. The bifurcation diagram ([Ca$^{2+}$] vs. $V_{PLC}$) exhibits a complex dynamical structure with more unstable and stable branches in relation to mitochondrial uptakes, releases, and MAM inclusions. The structure is particularly challenging because of the cascade of PDs and TR bifurcations. The dynamical structures are like these models [20, 36, 37, 48–50].

Nevertheless, by emphasizing ER-cytosolic exchange, SERCA pump, PMAC, external intakes as well as mitochondrial uptake, release, and MAMs, this work explains calcium oscillations in non-

excitable cells. Likewise, it addresses mixed IP$_3$ metabolism that generates a range of morphologies, such as baseline spikes, transient, sinusoidal, and simple to complex oscillations with low to high periods and frequencies. Therefore, here findings are in keeping with previous experimental research showing that agonists like acetylcholine (Ach), and vasopressin (VP) delivery lead in high frequency, sinusoidal baseline spikes, while cholecystokinin (cch), phenylephrine (PE) application results in low-frequency baseline spikes [5–7].

This model has few limitations. Here, we tried to develop a simple mathematical model that shows Ca$^{2+}$ dynamics physiologically accurate. This model is a well-mixed type, and the concentration of each species is homogeneous throughout. However, the Ca$^{2+}$ dynamics in non-excitable cells vary with space and time both. Thus, this model is limited to show the propagating of Ca$^{2+}$ waves from one region to another region of the cells. Also, to investigate Ca$^{2+}$ patterns through MAMs in the non-excitable cells; we use the direct Ca$^{2+}$ passage from the ER to the mitochondria. The more accurate model is to consider the microdomains near the connecting sights of the ER and the mitochondria. However, in the future, we will construct such kinds of models. This model is deterministic in nature. It does not provide any information regarding the stochastic aspects of Ca$^{2+}$ dynamics in the non-excitable cells.

Cell viability is dependent on the production of ATP via mitochondrial oxidative phosphorylation [51]. Moreover, the sustained rise of [Ca$^{2+}$] is shown to cause oxidative stress leading to the generation of excess ROS [52–56]. ROS are generated as byproducts of normal cellular respiration, particularly during the electron transport chain in the mitochondria. During the electron transport chain (ETC), electrons are transferred through Complex I, II, and III, and molecular oxygen O$_2$ serves as the final electron acceptor. Sometimes, during this process, some electrons can prematurely interact with O$_2$, leading to the formation of ROS. ROS includes molecules like superoxide radicals (O$_2$•−), hydrogen peroxide (H$_2$O$_2$), and hydroxyl radicals (•OH). Few mathematical models to understand these mechanisms are seen here [57–61]. Thus, it is important to understand the crosstalk between MAMs and ROS in non-excitable cells. But it is the avenue of future work.

## Declarations

### Use of AI tools

The author declares that he has not used Artificial Intelligence (AI) tools in the creation of this article.

### Data availability statement

There are no external data associated with this article.

### Ethical approval (optional)

The author states that this research complies with ethical standards. This research does not involve either human participants or animals.

### Consent for publication

Not applicable

### Conflicts of interest

The author declares that he has no conflict of interest.

### Funding

No funding was received for this research.

## Author's contributions

The author has written, read and agreed to the published version of the manuscript.

## References

[1] Berridge, M.J. Smooth muscle cell calcium activation mechanisms. *The Journal of Physiology,* 586(21), 5047-5061, (2008).[CrossRef]

[2] Südhof, T.C. Neurotransmitter release: the last millisecond in the life of a synaptic vesicle. *Neuron,* 80(3), 675-690, (2013).[CrossRef]

[3] Berridge, M., Lipp, P. and Bootman, M. Calcium signalling. *Current Biology,* 9(5), R157-R159, (1999).[CrossRef]

[4] Gerasimenko, J.V., Peng, S., Tsugorka, T. and Gerasimenko, O.V. $Ca^{2+}$ signalling underlying pancreatitis. *Cell Calcium,* 70, 95-101, (2018). [CrossRef]

[5] Bartlett, P.J., Cloete, I., Sneyd, J. and Thomas, A.P. $IP_3$-dependent $Ca^{2+}$ oscillations switch into a dual oscillator mechanism in the presence of PLC-linked hormones. *Iscience,* 23(5), 101062, (2020). [CrossRef]

[6] Yule, D.I. and Gallacher, D.V. Oscillations of cytosolic calcium in single pancreatic acinar cells stimulated by acetylcholine. *FEBS Letters,* 239(2), 358-362, (1988). [CrossRef]

[7] Petersen, O.H. Local calcium spiking in pancreatic acinar cells. *Ciba Foundation Symposium,* 188, 85-103, (1995).

[8] Raturi, A. and Simmen, T. Where the endoplasmic reticulum and the mitochondrion tie the knot: the mitochondria-associated membrane (MAM). *Biochimica et Biophysica Acta (BBA)-Molecular Cell Research,* 1833(1), 213-224, (2013). [CrossRef]

[9] Yang, M., Li, C., Yang, S., Xiao, Y., Xiong, X., Chen, W. et al. Mitochondria-associated ER membranes–the origin site of autophagy. *Frontiers in Cell and Developmental Biology,* 8, 595, (2020). [CrossRef]

[10] De Young, G.W. and Keizer, J. A single-pool inositol 1, 4, 5-trisphosphate-receptor-based model for agonist-stimulated oscillations in $Ca^{2+}$ concentration. *Proceedings of the National Academy of Sciences,* 89(20), 9895-9899, (1992). [CrossRef]

[11] Atri, A., Amundson, J., Clapham, D. and Sneyd, J. A single-pool model for intracellular calcium oscillations and waves in the Xenopus laevis oocyte. *Biophysical Journal,* 65(4), 1727-1739, (1993). [CrossRef]

[12] Dupont, G. and Swillens, S. Quantal release, incremental detection, and long-period $Ca^{2+}$ oscillations in a model based on regulatory $Ca^{2+}$-binding sites along the permeation pathway. *Biophysical Journal,* 71(4), 1714-1722, (1996). [CrossRef]

[13] Li, Y.X. and Rinzel, J. Equations for $InsP_3$ receptor-mediated $[Ca^{2+}]$ i oscillations derived from a detailed kinetic model: a Hodgkin-Huxley like formalism. *Journal of Theoretical Biology,* 166(4), 461-473, (1994). [CrossRef]

[14] Bezprozvanny, I. Theoretical analysis of calcium wave propagation based on inositol (1, 4, 5)-trisphosphate ($InsP_3$) receptor functional properties. *Cell Calcium,* 16(3), 151-166, (1994). [CrossRef]

[15] Cuthbertson, K.S.R. and Chay, T.R. Modelling receptor-controlled intracellular calcium oscillators. *Cell Calcium,* 12(2-3), 97-109, (1991). [CrossRef]

[16] Meyer, T. and Stryer, L. Molecular model for receptor-stimulated calcium spiking. *Proceedings of the National Academy of Sciences,* 85(14), 5051-5055, (1988). [CrossRef]

[17] Sneyd, J., Tsaneva-Atanasova, K., Bruce, J.I.E., Straub, S.V., Giovannucci, D.R. and Yule, D.I. A model of calcium waves in pancreatic and parotid acinar cells. *Biophysical Journal,* 85(3), 1392-1405, (2003). [CrossRef]

[18] Manhas, N. and Pardasani, K.R. Modelling mechanism of calcium oscillations in pancreatic acinar cells. *Journal of Bioenergetics and Biomembranes,* 46, 403-420, (2014). [CrossRef]

[19] Manhas, N., Sneyd, J. and Pardasani, K.R. Modelling the transition from simple to complex $Ca^{2+}$ oscillations in pancreatic acinar cells. *Journal of Biosciences,* 39, 463-484, (2014). [CrossRef]

[20] Manhas, N. and Anbazhagan, N. A mathematical model of intricate calcium dynamics and modulation of calcium signalling by mitochondria in pancreatic acinar cells. *Chaos, Solitons & Fractals,* 145, 110741, (2021). [CrossRef]

[21] Dupont, G., Falcke, M., Kirk, V. and Sneyd, J. *Models of Calcium Signalling* (Vol. 43). Springer: Switzerland, (2016). [CrossRef]

[22] Dupont, G., Swillens, S., Clair, C., Tordjmann, T. and Combettes, L. Hierarchical organization of calcium signals in hepatocytes: from experiments to models. *Biochimica et Biophysica Acta (BBA)-Molecular Cell Research,* 1498(2-3), 134-152, (2000). [CrossRef]

[23] Kummer, U., Olsen, L.F., Dixon, C.J., Green, A.K., Bornberg-Bauer, E. and Baier, G. Switching from simple to complex oscillations in calcium signaling. *Biophysical Journal,* 79(3), 1188-1195, (2000). [CrossRef]

[24] Ullah, G., Jung, P. and Machaca, K. Modeling $Ca^{2+}$ signaling differentiation during oocyte maturation. *Cell Calcium,* 42(6), 556-564, (2007). [CrossRef]

[25] Naik, P.A. and Pardasani, K.R. Three-dimensional finite element model to study calcium distribution in oocytes. *Network Modeling Analysis in Health Informatics and Bioinformatics,* 6, 16, (2017). [CrossRef]

[26] Naik, P.A. and Pardasani, K.R. Three-dimensional finite element model to study effect of RyR calcium channel, ER leak and SERCA pump on calcium distribution in oocyte cell. *International Journal of Computational Methods,* 16(01), 1850091, (2019). [CrossRef]

[27] Zhang, H., Zhang, S., Wang, W., Wang, K. and Shen, W. A mathematical model of the mouse atrial myocyte with inter-atrial electrophysiological heterogeneity. *Frontiers in Physiology,* 11, 972, (2020). [CrossRef]

[28] Greenstein, J.L. and Winslow, R.L. An integrative model of the cardiac ventricular myocyte incorporating local control of $Ca^{2+}$ release. *Biophysical Journal,* 83(6), 2918-2945, (2002). [CrossRef]

[29] Bers, D.M. Cardiac excitation–contraction coupling. *Nature,* 415, 198-205, (2002). [CrossRef]

[30] Bhattacharyya, R. and Jha, B.K. Analyzing fuzzy boundary value problems: a study on the influence of mitochondria and ER fluxes on calcium ions in neuron cells. *Journal of Bioenergetics and Biomembranes,* 56, 15-29, (2024). [CrossRef]

[31] Jethanandani, H., Jha, B.K. and Ubale, M. The role of calcium dynamics with amyloid beta on neuron-astrocyte coupling. *Mathematical Modelling and Numerical Simulation with Applications,* 3(4), 376-390, (2023). [CrossRef]

[32] Joshi, H., Yavuz, M. and Stamova, I. Analysis of the disturbance effect in intracellular calcium dynamic on fibroblast cells with an exponential kernel law. *Bulletin of Biomathematics,* 1(1), 24-39, (2023). [CrossRef]

[33] Ishii, K., Hirose, K. and Iino, M. $Ca^{2+}$ shuttling between endoplasmic reticulum and mitochondria underlying $Ca^{2+}$ oscillations. *EMBO Reports,* 7, 390-396, (2006). [CrossRef]

[34] Johnson, P.R., Dolman, N.J., Pope, M., Vaillant, C., Petersen, O.H., Tepikin, A.V. and Erdemli, G. Non-uniform distribution of mitochondria in pancreatic acinar cells. *Cell and Tissue Research,* 313, 37-45, (2003). [CrossRef]

[35] Tinel, H., Cancela, J.M., Mogami, H., Gerasimenko, J.V., Gerasimenko, O.V., Tepikin, A.V. and Petersen, O.H. Active mitochondria surrounding the pancreatic acinar granule region prevent spreading of inositol trisphosphate-evoked local cytosolic $Ca^{2+}$ signals. *The EMBO Journal,* 18, 4999-5008, (1999). [CrossRef]

[36] Dyzma, M., Szopa, P. and Kaźmierczak, B. Membrane associated complexes: new approach to calcium dynamics modelling. *Mathematical Modelling of Natural Phenomena,* 7(6), 167-186, (2012). [CrossRef]

[37] Marhl, M., Schuster, S. and Brumen, M. Mitochondria as an important factor in the maintenance of constant amplitudes of cytosolic calcium oscillations. *Biophysical Chemistry,* 71(2-3), 125-132, (1998). [CrossRef]

[38] Moshkforoush, A., Ashenagar, B., Tsoukias, N.M. and Alevriadou, B.R. Modeling the role of endoplasmic reticulum-mitochondria microdomains in calcium dynamics. *Scientific Reports,* 9, 17072, (2019). [CrossRef]

[39] Wacquier, B., Combettes, L., Van Nhieu, G.T. and Dupont, G. Interplay between intracellular $Ca^{2+}$ oscillations and $Ca^{2+}$-stimulated mitochondrial metabolism. *Scientific Reports,* 6, 19316, (2016). [CrossRef]

[40] Han, J.M. and Periwal, V. A mathematical model of calcium dynamics: Obesity and mitochondria-associated ER membranes. *PLoS Computational Biology,* 15(8), e1006661, (2019). [CrossRef]

[41] Doedel, E.J. AUTO: A program for the automatic bifurcation analysis of autonomous systems. In Proceedings, *10th Manitoba Conference on Numerical Mathematics and Computing*, (Vol. 30) pp. 265-284, Winnipeg, Canada, (1981, September).

[42] Sneyd, J. and Dufour, J.F. A dynamic model of the type-2 inositol trisphosphate receptor. *Proceedings of the National Academy of Sciences,* 99(4), 2398-2403, (2002). [CrossRef]

[43] Tsaneva-Atanasova, K., Yule, D.I. and Sneyd, J. Calcium oscillations in a triplet of pancreatic acinar cells. *Biophysical Journal,* 88(3), 1535-1551, (2005). [CrossRef]

[44] Politi, A., Gaspers, L.D., Thomas, A.P. and Höfer, T. Models of $IP_3$ and $Ca^{2+}$ oscillations: frequency encoding and identification of underlying feedbacks. *Biophysical Journal,* 90(9), 3120-3133, (2006). [CrossRef]

[45] Csordás, G., Várnai, P., Golenár, T., Roy, S., Purkins, G., Schneider, T. G. et al. Imaging interorganelle contacts and local calcium dynamics at the ER-mitochondrial interface. *Molecular Cell,* 39(1), 121-132, (2010). [CrossRef]

[46] Szopa, P., Dyzma, M. and Kaźmierczak, B. Membrane associated complexes in calcium dynamics modelling. *Physical Biology,* 10(3), 035004, (2013). [CrossRef]

[47] Li, X., Zhang, S., Liu, X., Wang, X., Zhou, A. and Liu, P. Important role of MAMs in bifurcation and coherence resonance of calcium oscillations. *Chaos, Solitons & Fractals,* 106, 131-140, (2018).

[CrossRef]

[48] Cloete, I., Bartlett, P.J., Kirk, V., Thomas, A.P. and Sneyd, J. Dual mechanisms of Ca$^{2+}$ oscillations in hepatocytes. *Journal of Theoretical Biology,* 503, 110390, (2020). [CrossRef]

[49] Ventura, A.C. and Sneyd, J. Calcium oscillations and waves generated by multiple release mechanisms in pancreatic acinar cells. *Bulletin of Mathematical Biology,* 68, 2205-2231, (2006). [CrossRef]

[50] LeBeau, A.P., Yule, D.I., Groblewski, G.E. and Sneyd, J. Agonist-dependent phosphorylation of the inositol 1, 4, 5-trisphosphate receptor: a possible mechanism for agonist-specific calcium oscillations in pancreatic acinar cells. *The Journal of General Physiology,* 113(6), 851-872, (1999). [CrossRef]

[51] Heiske, M., Letellier, T. and Klipp, E. Comprehensive mathematical model of oxidative phosphorylation valid for physiological and pathological conditions. *The FEBS Journal,* 284(17), 2802-2828, (2017). [CrossRef]

[52] Zhang, J., Wang, X., Vikash, V., Ye, Q., Wu, D., Liu, Y. and Dong, W. ROS and ROS-mediated cellular signaling. *Oxidative Medicine and Cellular Longevity,* 2016, 4350965, (2016). [CrossRef]

[53] Murphy, M.P. How mitochondria produce reactive oxygen species. *Biochemical Journal,* 417(1), 1-13, (2009). [CrossRef]

[54] Criddle, D.N. Reactive oxygen species, Ca$^{2+}$ stores and acute pancreatitis; a step closer to therapy?. *Cell Calcium,* 60(3), 180-189, (2016). [CrossRef]

[55] Chouchani, E.T., Pell, V.R., James, A.M., Work, L.M., Saeb-Parsy, K., Frezza, C. et al. A unifying mechanism for mitochondrial superoxide production during ischemia-reperfusion injury. *Cell Metabolism,* 23(2), 254-263, (2016). [CrossRef]

[56] Mazat, J.P., Devin, A. and Ransac, S. Modelling mitochondrial ROS production by the respiratory chain. *Cellular and Molecular Life Sciences,* 77, 455-465, (2020). [CrossRef]

[57] Quinlan, C.L., Orr, A.L., Perevoshchikova, I.V., Treberg, J.R., Ackrell, B.A. and Brand, M.D. Mitochondrial complex II can generate reactive oxygen species at high rates in both the forward and reverse reactions. *Journal of Biological Chemistry,* 287(32), 27255-27264, (2012). [CrossRef]

[58] Duong, Q.V., Levitsky, Y., Dessinger, M.J., Strubbe-Rivera, J.O. and Bazil, J.N. Identifying site-specific superoxide and hydrogen peroxide production rates from the mitochondrial electron transport system using a computational strategy. *Function,* 2(6), zqab050, (2021). [CrossRef]

[59] Manhas, N., Duong, Q.V., Lee, P., Richardson, J.D., Robertson, J.D., Moxley, M.A. and Bazil, J.N. Computationally modeling mammalian succinate dehydrogenase kinetics identifies the origins and primary determinants of ROS production. *Journal of Biological Chemistry,* 295(45), 15262-15279, (2020). [CrossRef]

[60] Manhas, N., Duong, Q.V., Lee, P. and Bazil, J.N. Analysis of mammalian succinate dehydrogenase kinetics and reactive oxygen species production. *bioRxiv,* 870501, (2019). [CrossRef]

[61] Chenna, S., Koopman, W.J., Prehn, J.H. and Connolly, N.M. Mechanisms and mathematical modeling of ROS production by the mitochondrial electron transport chain. *American Journal of Physiology-Cell Physiology,* 323(1), C69-C83, (2022). [CrossRef]

Mathematical Modelling and Numerical Simulation with Applications (MMNSA)
(https://dergipark.org.tr/en/pub/mmnsa)